

# A new sample of X-ray selected narrow emission-line galaxies.

## I. The nature of optically elusive AGN.

E. Pons and M. G. Watson

Department of Physics & Astronomy, University of Leicester, Leicester, LE1 7RH, UK

Received 24 March 2014 / Accepted 15 July 2014

### ABSTRACT

Using the 3XMM catalogue of serendipitous X-ray sources, and the SDSS-DR9 spectroscopic catalogue, we have obtained a new sample of X-ray selected narrow emission line galaxies. The standard optical diagnostic diagram and selection by hard X-ray luminosity expose a mismatch between the optically-based and X-ray-based classifications. The nature of these misclassified “elusive” AGN can be understood in terms of their broader X-ray and optical properties and leads to a division of this sub-sample into two groups. A little more than half are likely to be narrow-line Seyfert 1s (NLS1s), so misclassified because of the contribution of the Broad Line Region (BLR) to their optical spectra. The remainder have some of the properties of Seyfert 2 (Sy2) AGN; their optical elusiveness can be explained by optical dilution from the host galaxy plus a star-formation contribution and by their underluminous optical emission due to low accretion rates. Because some of the Sy2 sources have very low accretion rates, are unabsorbed, plus the fact that they lack broad optical emission lines, they are good candidates to be *True* Sy2 AGN.

**Key words.** Galaxies: active – Galaxies: Seyfert – X-rays: galaxies

### 1. Introduction

There is strong observational evidence that most, if not all, massive galaxies ( $M_* > 10^{10} - 10^{12} M_\odot$ ) in the nearby Universe host a central supermassive black hole (SMBH; Kormendy & Richstone (1995)). Central black holes are less common in low-mass systems, but have still been identified in some low mass and dwarf galaxies (Filippenko & Ho 2003; Barth et al. 2004; Reines et al. 2011). The central sources in galaxies are observed as active galactic nuclei (AGN) as the SMBH grows through a phase of significant mass accretion.

With large surveys at different wavelengths, various criteria can be used to identify AGN. In the optical, type 2 AGN can be distinguished from star-forming (SF) galaxies on the basis of their emission lines. The most commonly used diagnostic for large sample of galaxies is the BPT diagram introduced by Baldwin et al. (1981). This considers the emission-line ratios to probe the source of excitation. In the case of photoionization from young and massive O stars (in star-forming galaxies), the low ionization transitions (i.e. the collisionally-excited lines) [NII], [SII], [OIII] and especially [OI] are very weak relative to the Balmer recombination lines. In contrast, for photoionization from an accretion disc around a SMBH, the collisionally-excited lines will be stronger because the photons from an AGN extend to higher energy.

However, some X-ray selected AGN, selected by their hard X-ray luminosity, will not be classified as AGN by their optical emission line properties. This class of sources has been given a variety of names such as “elusive” AGN<sup>1</sup> (Caccianiga et al. 2007), “optically dull” AGN (Elvis et al. 1981; Trump

et al. 2009) or also “X-ray bright, optically normal galaxies” (XBONG; Comastri et al. (2002)). Such galaxies are particularly interesting because, despite their luminous X-ray emission, they lack clear optical signatures of an AGN. Previous studies have shown that many of these sources are not so special but are indeed normal type 2 AGN diluted by a bright host (Moran et al. 2002; Caccianiga et al. 2007); however about 10-20% are undiluted (La Franca et al. 2002) and so dilution may not be the cause of all optically dull AGN. Another possibility is that the optical emission of elusive AGN has been rendered “invisible” by obscuration which may be caused by optically-thick gas clouds covering the nuclear source, as suggested by Comastri et al. (2002), or instead by extranuclear gas and dust in the host galaxy (Rigby et al. 2006). Alternatively, a fraction of elusive AGN are intrinsically optically weaker than other AGN (Trump et al. 2009) and can be characterised by unusual properties such as weak emission from the accretion disk (e.g. radiatively inefficient accretion flow RIAF, Yuan & Narayan (2004)). Finally more recent work by Castelló-Mor et al. (2012) proposes that the optical misclassification of X-ray bright AGN through emission lines may be due to the contamination of the narrow-line galaxy samples by narrow-line Seyfert 1 (NLS1), a subclass of unobscured AGN which have narrower line width (usually between 500 and 2000 km.s<sup>-1</sup>) and a [OIII]/H $\beta$  line ratio smaller than 3 (Boller et al. 1996; Botte et al. 2004).

In this paper we investigate a new sample of Seyfert 2 (Sy2) galaxies with conflicting X-ray and optical classifications. After identifying possible NLS1, we consider three explanations for optical dullness of the remaining Sy2 galaxies in the sample: (1) obscuration by an dusty torus (Compton-thick AGN,  $N_H > 10^{24} \text{ cm}^{-2}$ ); (2) optical dilution from the host galaxy star-light; (3) weak emission from the accretion disc related low accretion rates.

<sup>1</sup> In this paper, the term “elusive” AGN refers to objects with X-ray emission like an AGN but optical emission line ratios like a star-forming galaxy.

Some of the AGN in our sample may belong to a more exotic class of AGN which are inconsistent with the predictions of the Unified Model (Antonucci 1993; Urry & Padovani 1995). According to this scheme, AGN are classified into two classes based on the presence (type 1) or absence (type 2) of broad emission lines in their optical spectra. This means that the central black hole (BH) is viewed directly (type 1) or is obscured by a dusty torus (type 2). However, type 2 AGN without an hidden broad line region (BLR) have been found (Bianchi et al. 2012); these are not predicted by the model. These sources, often called *True Seyfert 2*, may be observed while accreting at low Eddington rates, in agreement with models which predict that the BLR disappears below a certain accretion rate threshold (Yuan 2007) and the absence of observed broad-line AGN below a limiting accretion rate (corresponding to an Eddington ratio smaller than  $10^{-2}$ ) (Trump et al. 2011).

The aim of this paper is to understand the nature of a new sample of AGN which have conflicting properties in the optical and X-ray band. This sample also allows us to find peculiar AGN with unexpected properties. The paper is structured as follows: section 2 describes the source selection; the X-ray and optical properties are detailed in section 3; and the section 4 discusses the most likely explanations for optical dullness.

## 2. Narrow emission-line galaxies sample

### 2.1. Source selection

The 3XMM catalogue of serendipitous X-ray sources (Watson et al. 2014; in preparation) is currently the largest X-ray catalogue containing over 370,000 discrete entries drawn from over 7000 pointed XMM-Newton observations covering around 2% of the sky. About 45% of 3XMM catalogue sources lie in the region covered by the Sloan Digital Sky Survey (SDSS). To create our sample of X-ray selected galaxies we carried out a positional cross-match of the 3XMM catalogue with SDSS-DR9, the ninth SDSS data release, focusing exclusively on galaxies with SDSS spectroscopy ( $\sim 1,690,000$  objects). This allows us to create a large sample of sources with useful X-ray and optical data.

From SDSS we selected galaxies with a spectroscopic classification of “GALAXY” or “QSO” and which are “science primary” objects (i.e. those that have the best available spectra). The cross-matched X-ray/optical sample is obtained by cross-correlating the SDSS spectroscopic galaxies sub-sample with the 3XMM catalogue. SDSS galaxies are considered as **potential** counterparts to the X-ray sources if the separation between the optical and X-ray positions is smaller than  $10''$  and for which the normalised separation (i.e. the ratio of the separation to the X-ray position error) is smaller than 4 (Pineau et al. 2011). Because we restrict our sample to SDSS spectroscopic objects, which are significantly brighter and thus have lower sky density than galaxies in the SDSS photometric catalogue, spurious matches become negligible even with these generous limits. In addition, X-ray sources are required to be point-like (3XMM catalogue parameter SC\_EXTENT < 5; thus removing galaxy clusters) and to have a relatively high detection significance (catalogue parameter SC\_DET\_ML > 15). This results, at this stage, in a cross-matched catalogue of about 4900 X-ray objects with SDSS spectroscopic data.

From this sample, narrow emission-line galaxies are selected by requiring the full-width at half maximum (FWHM) of the Balmer lines to be smaller than  $1000 \text{ km.s}^{-1}$  (e.g. Caccianiga et al. 2008); this threshold rejects all *bona fide* broad-line objects and reduces the contamination by conventional Narrow Line

Seyfert 1 (NLS1). Narrow emission-line galaxies represent 31% of the whole cross-matched catalogue, corresponding to 1555 sources.

Additional derived products for galaxies in the SDSS spectroscopic database are available from the MPA-JHU group. These are the GALPESPEC measurements (described in Brinchmann et al. (2004); Kauffmann et al. (2003b); Tremonti et al. (2004)). The derived spectral products include emission line fluxes corrected for Galactic reddening (using the maps of Schlegel et al. (1998)). In addition, through fitting of the observed spectrum with galaxy spectra models, the derived products provide estimates of emission line strengths after subtraction of stellar absorption line components. This is important because the SDSS aperture of the spectroscopic fibre is  $3''$  and thus the spectra include not only the nucleus but have also host galaxy contribution. Moreover, using stellar population models, the derived products include a variety of galaxy parameters (e.g. stellar masses, stellar and gas kinematics, velocity dispersions ...). We choose to keep only sources for which these improved derived spectral products were available. Furthermore we removed from our sample those galaxies which are, SDSS “X-ray targets” (those selected from ROSAT, Chandra and XMM catalogues), together with objects from the SDSS BOSS sample (most of which, in our sample, are X-ray selected or are selected because they other particular properties). Moreover sources which are the targets of XMM-Newton observations are also removed. We have made this selection because these SDSS and XMM “targets” would represent a biased subsample.<sup>2</sup> After the new selections have been applied the final sample consists of 1514 objects, corresponding to 97% of the narrow emission-line galaxies.

Finally, to have a trustworthy sample classification, galaxies are only considered if they have a reasonable quality optical spectrum (signal to noise ratio of the whole spectrum  $S/N > 3$ ) and a redshift  $z < 0.4$  (so that all of the four lines  $H\beta$ ,  $[\text{OIII}]\lambda 5007$ ,  $H\alpha$  and  $[\text{NII}]\lambda 6584$  are covered). We further require that these lines are in emission with a reliable measurement; specifically the line ratios  $[\text{OIII}]/H\beta$  and  $[\text{NII}]/H\alpha$  must be three times larger than the error on the ratio.

Using these criteria, the final sample of X-ray selected narrow-emission line galaxies (NELGs) includes 797 X-ray sources with good SDSS spectroscopy and a median redshift of 0.15.

### 2.2. Classification

#### 2.2.1. Optical classification

The BPT diagnostic diagram is used to classify the NELGs sample on the basis of their optical emission properties. The classification scheme that best distinguishes between AGN and star-forming galaxies uses the  $[\text{OIII}]/H\beta$  vs.  $[\text{NII}]/H\alpha$  emission-line ratios (Stasińska et al. 2006). The other main virtues of this scheme are that the lines used are relatively strong, lie in an easily accessible region of the optical spectrum and the line ratios are relatively insensitive to reddening because of their close separation in wavelength.

Two demarcation lines are used here for the classification. The first is the theoretical division from Kewley et al. (2001, hereafter Ke01), which uses a combination of photoionization and stellar population synthesis models to place a theoretical

<sup>2</sup> An unbiased sample is required for future analysis using the same dataset.

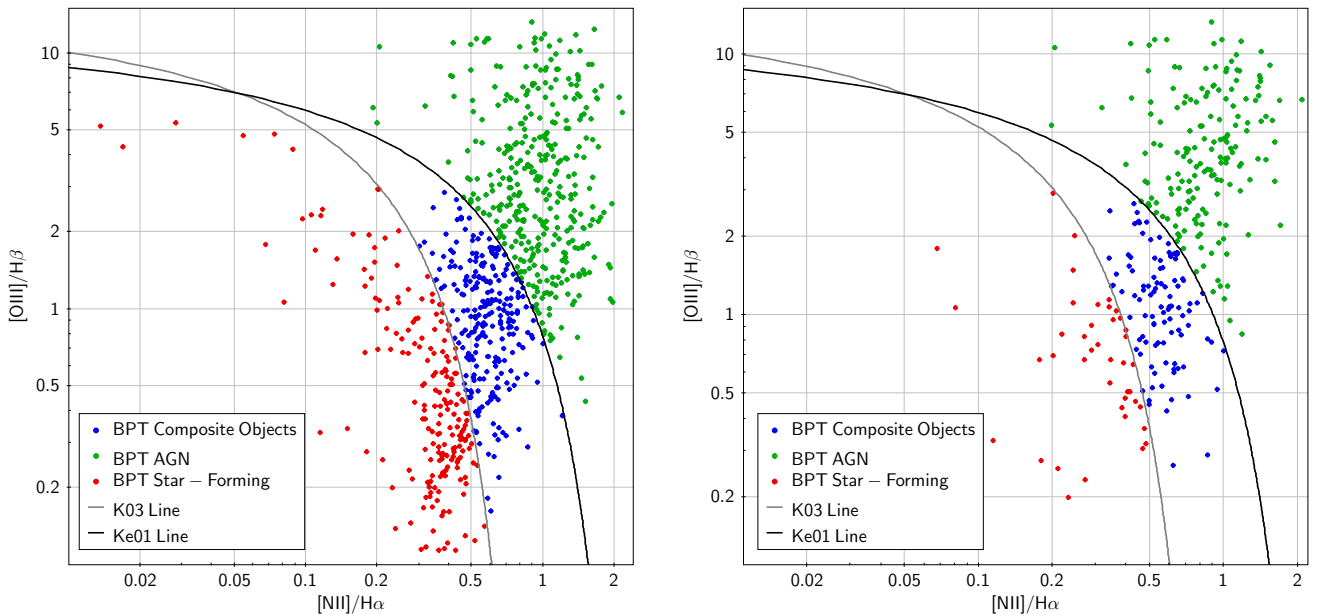


**Fig. 1.** BPT emission line diagnostic diagrams. The K03 line in grey separates the SF galaxies and composite object regions, while the Ke01 demarcation line in black distinguishes between optically-classified AGN and composite objects. **Left panel:** NELG sample which consists of 797 sources (45% of BPT-AGN (green symbols), 31% composite objects (blue symbols) and 24% in the SF region (red symbols)). **Right panel:** NELG sample with high hard X-ray luminosity ( $L_{HX} > 10^{42}$  erg.s $^{-1}$ ). There are 172 sources (54% of the sample) classified as BPT-AGN (green symbols), 103 sources (blue symbols) classified as composite objects and 41 sources (13%) in the SF region of the diagram (red symbols; our elusive AGN).

conservative lower limit on the true number of AGN:

$$\log\left(\frac{[OIII]\lambda 5007}{H\beta}\right) = \frac{0.61}{\log\left(\frac{[NII]\lambda 6584}{H\alpha}\right) - 0.47} + 1.19$$

We also use an empirical line ratio based on the data from Kauffmann et al. (2003a, hereafter K03) that places a conservative limit on the true number of SF galaxies:

$$\log\left(\frac{[OIII]\lambda 5007}{H\beta}\right) = \frac{0.61}{\log\left(\frac{[NII]\lambda 6584}{H\alpha}\right) - 0.05} + 1.3$$

The objects that lie below the K03 line are optically classified as SF galaxies (BPT-SF), the ones that are above the Ke01 line are classified as AGN (BPT-AGN). The objects that lie between these two lines are called Composite objects because their optical spectra may include a contributions from both star-formation and an active nucleus. The classification for the whole NELG sample is shown in the left panel of the Fig. 1.

## 2.2.2. X-ray classification

An alternative way of classifying galaxies as AGN uses an empirical X-ray luminosity threshold. The rest-frame hard X-ray luminosity in the 2 - 10 keV band ( $L_{HX}$ ) is computed from the measured flux, making the simple assumption that the X-ray spectrum has a power-law form with a photon index  $\Gamma$  of 1.7. The luminosity estimated this way is relatively insensitive to changes in the assumed photon index. Choosing sources with  $L_{HX} > 10^{42}$  erg.s $^{-1}$  is known to remove galaxies with X-ray emission powered by mechanisms other than nuclear activity (Fabbiano 1989; Mushotzky 2004). This empirical limit works because for a star-forming galaxy to have such a high X-ray luminosity requires a star formation rate (SFR) of at least  $200 M_{\odot} \cdot \text{yr}^{-1}$  (e.g. relation from Ranalli et al. (2003);  $L_{HX} = SFR[M_{\odot} \cdot \text{yr}^{-1}] \cdot 5 \cdot 10^{39}$  erg.s $^{-1}$ ). Such a high SFR corresponds

to that of powerful Ultra Luminous Infrared Galaxies (ULIRGs;  $SFR_{min,ULIRG} \sim 100 M_{\odot} \cdot \text{yr}^{-1}$ ), objects which have a low space density, and thus are unlikely to be a significant contaminant at  $z < 0.4$ . So selection with a threshold  $L_{HX} > 10^{42}$  erg.s $^{-1}$  should produce a sample that only contains AGN. However, among the 316 NELGs with X-ray luminosity above this threshold, there remain 41 sources (13%) that are optically classified as SF galaxies. We refer to these as elusive AGN (see Fig.1, right panel).

The SFR provide in the SDSS GALSPEC catalogue ( $SFR_{SDSS}$ )

## 3. X-ray vs. optical properties

In this section we discuss the X-ray and optical properties of the elusive AGN.

### 3.1. X-ray vs. [OIII] luminosity

We compare the hard X-ray and [OIII] luminosities using [OIII] luminosities which are corrected for intrinsic absorption using the Balmer decrement, assuming an intrinsic ratio  $(H\alpha/H\beta)_0$  of 3.1 in the NLR (see Osterbrock & Ferland 2006) and a  $H\beta/H\alpha$  colour index for extinction  $\alpha = 2.94$  (Bassani et al. 1999):

$$f_{corr} = f_{obs} \cdot \left(\frac{H\alpha/H\beta}{(H\alpha/H\beta)_0}\right)^{\alpha}$$

Compared to the BPT-AGN and composite objects in the sample, the elusive AGN have a mean thickness parameter  $T$  ( $T = L_{HX}/L_{[OIII]}$ ) which is larger ( $\log_{10} T \sim 2.1$ ) than the other sources ( $\log_{10} T \sim 1.5$ ); but still in the typical range of values for Seyfert galaxies ( $-1 \lesssim \log_{10} T \lesssim 2$ ; Bassani et al. (1999)) (see Fig.2). This is consistent with the idea that some of the AGN in our sample could have anomalously low [OIII] flux (see also Trouille & Barger 2010).

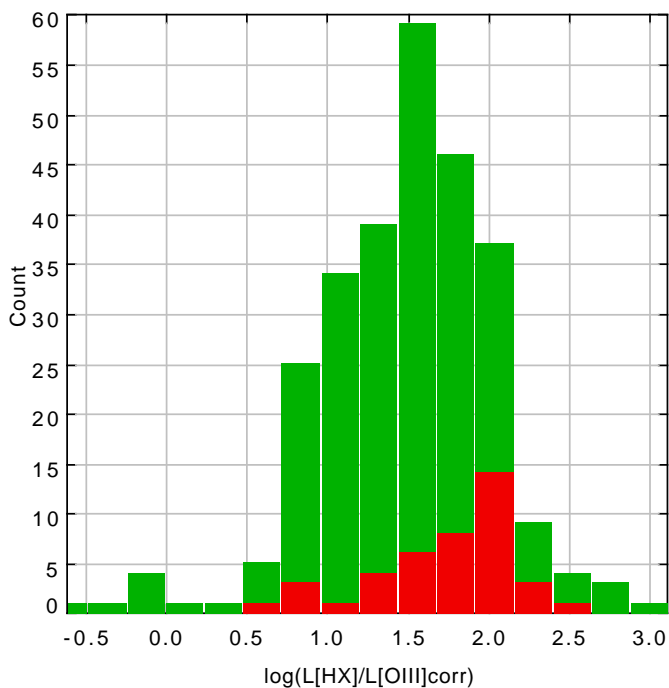


**Fig. 2.**  $L_{\text{HX}}/L_{[\text{OIII}],\text{corr}}$  distribution for the BPT-AGN and composite objects (green) and the elusive AGN (red). The latter sources have a higher mean ratio compared to the other AGN in the sample.

### 3.2. Emission line width vs. X-ray spectral information

A crude indicator of the X-ray spectral properties can be deduced from the Hardness Ratio (HR) diagram (also called X-ray colour-colour diagram) which simply compares count rates in adjacent energy bands. The HR is defined in terms of the observed counts rates  $R$  in energy bands  $n$  and  $n + 1$  as follows:

$$HR_n = (R_{n+1} - R_n) / (R_{n+1} + R_n) \quad \text{for } n = 1 - 4$$

where the five energy bands are 0.2 – 0.5 keV, 0.5 – 1.0 keV, 1.0 – 2.0 keV, 2.0 – 4.5 keV and 4.5 – 12 keV.

The HR3 vs. HR2 diagram, shown in Fig. 3, gives an approximate indicator of the intrinsic X-ray spectral shape and is also sensitive to the level of absorption. AGN with intrinsic absorption have a X-ray spectrum much harder than an unabsorbed one because the soft X-ray emission is differentially attenuated by the absorber. The dominant source of variation in the HR values is absorption (see Wang et al. 2004, Fig. 2). So an unabsorbed X-ray spectrum has HR2 and HR3 values lower than an absorbed one for a wide range of assumed continuum shapes. A typical type 1 AGN has a HR2 value  $\sim 0$  and  $HR3 < 0$ ; an increase in absorption above  $10^{22} \text{ cm}^{-2}$  would increase the HR values to  $HR2 \sim 0.4$  and  $HR3 \sim 0$  (see Watson et al. 2009, Fig. 12). About 73% of the elusive AGN have low hardness ratios ( $HR2 < 0.4$  and  $HR3 < 0$ ), consistent with being unabsorbed or having low absorption.

The selected narrow-line AGN, even with a threshold of  $1000 \text{ km}^{-1}$  for the FWHM of the Balmer lines, could still be contaminated by NLS1. Indeed it has previously been noted that NLS1 can lie in the star-forming region of the BPT diagram (Osterbrock & Pogge 1985; Rodríguez-Ardila et al. 2000) and that the lower end of their FWHM distribution can extend down to  $500 - 600 \text{ km s}^{-1}$  (Boller et al. 1996).

If we divide our elusive sample into “broad” line and “narrow” line sub-samples (hereafter referred as *narrow* and *broad* sub-samples respectively) by taking a

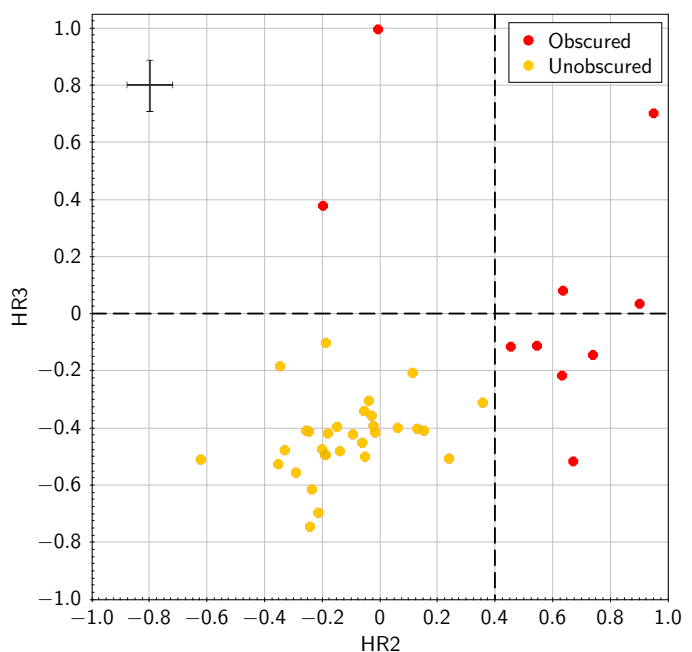


**Fig. 3.** X-ray colour-colour diagram (or HR diagram) of the elusive AGN. Gives a crude indication of the intrinsic X-ray spectral shape and level of absorption. The majority of the sources have a low HR (in yellow) consistent with being unabsorbed or having low absorption column density  $N_H \lesssim 10^{22} \text{ cm}^{-2}$ . The errors for both HR2 and HR3 range from about 0.01 to 0.2, with a mean values of respectively 0.08 and 0.09. The size of the typical (mean) errors is indicated by the black error-bars shown in the top left of the diagram.

$\text{FWHM}_{\text{Balmer}}$  limit of  $600 \text{ km.s}^{-1}$ , the 19 broader line sources ( $\text{FWHM}_{\text{Balmer}} > 600 \text{ km.s}^{-1}$ ), all have a low HR (indicating low absorption) and so are candidates to be NLS1. On the other hand the nature of the sources with lower velocity widths is at this point unclear and only 41% of them show clear signs of absorption (i.e. have high HR; the others “narrow” sources with low HR are referred as the *unobscured narrow* sub-sample). Most of them also have a velocity width smaller than  $350 \text{ km s}^{-1}$  corresponding to characteristic values of host galaxy lines and so do not seem to be dominated by an AGN in the optical. Five sources have velocity width broader than expected for a host galaxy, so may be AGN dominated, but still below the broad limit chosen to distinguish between NLS1 and Sy2 ( $\text{FWHM}_{\text{balmer}} \sim 400 - 600 \text{ km.s}^{-1}$ ) (see Fig. 4). These five sources have an ambiguous classification based on their Balmer velocity line width only; they can be classical AGN dominated X-ray Sy2 or NLS1 but with very low line widths compared to common sources of this class. The separation between the *broad* and *narrow* sub-samples for these sources require further analysis and will be discussed in section 3.4. At this stage possible NLS1 in the elusive sample are assumed to have line FWHM greater than  $600 \text{ km.s}^{-1}$  and so belong to the *broad* sub-sample.

### 3.3. X-ray spectral analysis

An X-ray spectral analysis of the elusive AGN has been carried out based on the XMM-Newton EPIC data and using XSPEC (version 12.8.0). The source parameters and classification are given Table 1.

For the sources with more than 500 counts in the three EPIC cameras combined, spectra are already extracted as pipeline data products associated with the 3XMM catalogue. In this case, we



**Table 1.** Observational parameters and classification of the elusive sources

3XMM SRCID	IAU Name (3XMM ...)	OBSID	$t_{exp}$ (ks)	EPIC-pn counts	$N_{H,gal}$ ( $\cdot 10^{20} \text{ cm}^{-2}$ )	Sub-sample <sup>(1)</sup>	$z$ <sup>(2)</sup>	$L_{HX}$ ( $\cdot 10^{42} \text{ erg.s}^{-1}$ )	$M_r$ <sup>(3)</sup> (mag)
1780	J121048.0+393745	0112830201	58.9	$331 \pm 14^\circ$	2.13	$\mathcal{N}1$ ( $n\mathcal{N}1$ )	0.20	$6.17 \pm 1.21$	-22.3
3161	J094540.4+094749	0150970301	23.4	$154 \pm 15^*$	2.50	$\mathcal{N}$ ( $n\mathcal{N}$ )	0.16	$6.44 \pm 1.56$	-22.2
3173	J103342.7+392926	0506440101	87.8	$498 \pm 26^\circ$	1.31	$\mathcal{N}$ ( $n\mathcal{N}$ )	0.07	$1.99 \pm 0.31$	-21.5
7207	J095921.2+024030	0302351601	30.5	$2017 \pm 56$	1.76	$\mathcal{B}$ ( $n\mathcal{B}$ )	0.26	$16.97 \pm 1.45$	-23.0
18567	J001804.8-005141	0403760701	27.1	$1271 \pm 39$	2.99	$\mathcal{B}$ ( $n\mathcal{B}$ )	0.19	$7.27 \pm 1.29$	-19.5
18747	J135810.3+653300	0305920601	12.0	$463 \pm 26$	1.38	$\mathcal{B}$ ( $n\mathcal{B}$ )	0.23	$8.84 \pm 1.65$	-21.8
* 28357	J134834.9+263109	0097820101	34.3	$42599 \pm 218$	1.21	$\mathcal{B}$ ( $n\mathcal{B}$ )	0.06	$8.24 \pm 0.16$	-20.9
28899	J094240.9+480017	0201470101	11.9	$393 \pm 22$	1.19	$\mathcal{N}1$ ( $n\mathcal{B}$ )	0.20	$2.61 \pm 1.22$	-21.1
29911	J100234.8+024253	0203360101	26.0	$416 \pm 25$	1.78	$\mathcal{B}$ ( $n\mathcal{B}$ )	0.20	$2.79 \pm 0.48$	-21.4
36405	J231858.2+000621	0305600601	16.0	$169 \pm 15^*$	3.90	$\mathcal{B}$ ( $n\mathcal{B}$ )	0.32	$12.84 \pm 7.03$	-21.8
47793	J112758.2+583558	0112810101	20.6	$123 \pm 15^*$	0.91	$\mathcal{N}1$ ( $n\mathcal{N}1$ )	0.18	$1.32 \pm 0.53$	-21.9
88476	J080455.5+241124	0203280201	6.3	$311 \pm 19$	3.92	$\mathcal{N}1$ ( $n\mathcal{B}$ )	0.14	$4.53 \pm 1.22$	-22.0
93560	J015727.2-004041	0303110101	3.5	$255 \pm 20^*$	2.61	$\mathcal{B}$ ( $n\mathcal{B}$ )	0.39	$47.50 \pm 21.50$	-22.3
93640	J015804.7-005222	0303110101	3.4	$356 \pm 22^*$	2.50	$\mathcal{N}1$ ( $n\mathcal{N}1$ )	0.08	$1.18 \pm 0.50$	-19.7
115294	J004335.9+001455	0303562201	4.4	$155 \pm 14^*$	1.72	$\mathcal{B}$ ( $n\mathcal{B}$ )	0.11	$5.32 \pm 2.73$	-21.4
120992	J002253.2+001659	0407030101	27.0	$207 \pm 20^*$	2.75	$\mathcal{N}$ ( $n\mathcal{N}$ )	0.21	$13.31 \pm 2.42$	-21.4
126294	J011929.0-000839	0605391101	7.3	$596 \pm 26^\circ$	3.35	$\mathcal{B}$ ( $n\mathcal{B}$ )	0.09	$8.95 \pm 2.30$	-20.8
155684	J030634.0-001355	0201120101	12.1	$145 \pm 19^*$	6.14	$\mathcal{N}$ ( $n\mathcal{N}$ )	0.22	$1.71 \pm 0.71$	-22.2
155872	J030705.8-000009	0142610101	40.3	$1355 \pm 42$	6.27	$\mathcal{B}$ ( $n\mathcal{B}$ )	0.27	$10.20 \pm 1.62$	-21.0
266064	J212929.6+000102	0093030201	34.7	$178 \pm 20^*$	3.67	$\mathcal{N}$ ( $n\mathcal{N}$ )	0.13	$1.95 \pm 0.27$	-21.4
266125	J213026.2-000204	0093030201	34.6	$144 \pm 22^*$	3.65	$\mathcal{N}1$ ( $n\mathcal{N}1$ )	0.14	$1.77 \pm 0.89$	-21.7
275370	J104549.6+213106	0128531601	76.5	$62 \pm 13^*$	1.83	$\mathcal{N}1$ ( $n\mathcal{N}1$ )	0.14	$1.17 \pm 0.62$	-21.6
277671	J110738.9+520644	0304071201	5.9	$167 \pm 16^*$	0.94	$\mathcal{N}$ ( $n\mathcal{N}$ )	0.18	$17.49 \pm 4.78$	-22.1
282027	J102812.6+293223	0301650401	7.8	$115 \pm 13^*$	1.91	$\mathcal{B}$ ( $n\mathcal{B}$ )	0.29	$16.01 \pm 12.10$	-21.7
291676	J115648.6+064753	0301651801	4.0	$305 \pm 19^*$	1.14	$\mathcal{N}1$ ( $n\mathcal{B}$ )	0.15	$3.18 \pm 2.85$	-22.2
294033	J111443.6+525834	0143650901	3.7	$885 \pm 31$	0.97	$\mathcal{B}$ ( $n\mathcal{B}$ )	0.08	$3.60 \pm 0.86$	-21.4
297574	J112405.1+061248	0103863201	5.1	$896 \pm 33$	4.61	$\mathcal{B}$ ( $n\mathcal{B}$ )	0.27	$28.25 \pm 4.80$	-22.5
303293	J091440.9+435716	0604680201	14.3	$148 \pm 18^*$	1.45	$\mathcal{N}1$ ( $n\mathcal{N}1$ )	0.19	$2.74 \pm 1.36$	-22.3
305003	J084058.1+383300	0502060201	16.1	$991 \pm 34$	3.15	$\mathcal{N}1$ ( $n\mathcal{N}1$ )	0.12	$3.19 \pm 0.61$	-21.5
321587	J094057.1+032400	0306050201	22.3	$5213 \pm 76$	2.99	$\mathcal{B}$ ( $n\mathcal{B}$ )	0.06	$4.91 \pm 0.32$	-20.8
324308	J134235.6+262533	0108460101	25.6	$1002 \pm 33^\circ$	1.03	$\mathcal{B}$ ( $n\mathcal{B}$ )	0.06	$3.78 \pm 0.44$	-20.9
337999	J151128.9+561317	0670650401	7.4	$655 \pm 29^*$	1.38	$\mathcal{N}1$ ( $n\mathcal{B}$ )	0.15	$16.48 \pm 2.91$	-22.4
339379	J151525.0+042146	0653810601	7.6	$263 \pm 22^*$	3.57	$\mathcal{N}1$ ( $n\mathcal{N}1$ )	0.10	$3.91 \pm 0.54$	-21.5
341733	J141449.5+361240	0148620101	13.9	$1217 \pm 17$	1.01	$\mathcal{B}$ ( $n\mathcal{B}$ )	0.18	$10.59 \pm 1.19$	-21.4
348033	J123155.5+200333	0301450201	24.1	$67 \pm 11^*$	2.58	$\mathcal{N}$ ( $n\mathcal{N}$ )	0.11	$1.51 \pm 0.74$	-20.8
350309	J123748.5+092323	0504100601	17.6	$2224 \pm 51$	1.47	$\mathcal{B}$ ( $n\mathcal{B}$ )	0.12	$11.24 \pm 2.14$	-21.7
350410	J123719.3+114915	0112840101	14.5	$247 \pm 20^*$	2.83	$\mathcal{N}$ ( $n\mathcal{N}$ )	0.11	$2.26 \pm 0.34$	-20.7
354458	J121613.0-032025	0305800701	3.8	$136 \pm 14^*$	2.66	$\mathcal{N}$ ( $n\mathcal{N}$ )	0.13	$2.36 \pm 0.73$	-21.6
356567	J122349.5+072657	0205090101	21.5	$1288 \pm 39$	1.70	$\mathcal{N}1$ ( $n\mathcal{B}$ )	0.07	$1.82 \pm 0.33$	-21.6
358675	J121814.8+142601	0147610101	13.4	$456 \pm 24$	2.87	$\mathcal{B}$ ( $n\mathcal{B}$ )	0.13	$4.45 \pm 0.76$	-20.1
369702	J125821.3+013158	0658400601	14.0	$2373 \pm 52$	1.45	$\mathcal{B}$ ( $n\mathcal{B}$ )	0.16	$2.51 \pm 0.64$	-21.1

**Notes.** <sup>(\*)</sup> This source is not an XMM-Newton target, nevertheless, detailed analysis of its serendipitous XMM data is presented by Zoghbi et al. (2008) (see also Upper panel of Fig.5). <sup>(1)</sup> The sub-sample names  $\mathcal{B}$ ,  $\mathcal{N}$  and  $\mathcal{N}1$  correspond respectively to the *broad*, *narrow* and *unobscured narrow* sub-samples. The classification given in brackets is discussed later, in section 3.4. <sup>(2)</sup> The errors on the redshift  $z$  and the absolute  $r$  magnitude  $M_r$  are not shown because they are smaller than 1%. <sup>(3)</sup> EPIC-MOS counts; because there is no pn data for these sources. <sup>(\*)</sup> Total EPIC counts.

use the EPIC-pn spectra from the PPS files with the corresponding latest version of the calibration files (SAS 11.0).

For the other sources, the raw observation data files (ODF) were reduced and analysed using the Science Analysis System (SAS) tool (xmmselect version 2.65.2) using standard techniques. The spectral data were extracted from an optimised circular region, and the corresponding background files from a nearby circular region free of sources. Because of the low number of counts, to improve the analysis, the EPIC-pn and EPIC-MOS spectra are analysed simultaneously with a constant coefficient inserted to model calibration uncertainties between the detectors (coefficient fixed to 1 for the pn and allowed to vary

for the MOS data). In the few cases for which pn spectra are not available, we use the MOS data.

The spectral data are grouped with a minimum of 20 counts per bin in order to use the  $\chi^2$  fit statistics. However, for the lowest quality spectra, data are grouped with only one count per bin and, in this case, we use Cash statistics (Cash 1979).

The classical model of the X-ray spectrum of an AGN is a power-law modified by absorption, with in some cases a soft X-ray excess (usually present in NLS1 spectra) and a Fe  $K\alpha$  emission line around 6.4 keV. The absorbed power-law comes from the Comptonization of photons from the accretion disc by a corona of hot material. The soft X-ray excess may

**Table 2.** X-ray spectral analysis results.

SRCID	Model	$\Gamma$	kT (keV)	$N_H$ ( $\cdot 10^{22}$ cm $^{-2}$ ) <sup>(1)</sup>	Red- $\chi^2$	goodness	P(ftest)	FeK	Sub-sample <sup>(2)</sup>
7207	(2)	2.40 <sup>+0.45</sup> <sub>-0.41</sub>	0.12 <sup>+0.08</sup> <sub>-0.04</sub>	0.12 <sup>+0.21</sup> <sub>-0.11</sub>	1.218	31%	0.019	✓	$\mathcal{B}$ ( $n\mathcal{B}$ )
18567	(2)	2.19 <sup>+0.27</sup> <sub>-0.26</sub>	0.10 <sup>+0.02</sup> <sub>-0.02</sub>	<0.01	1.176	44%	0.004		$\mathcal{B}$ ( $n\mathcal{B}$ )
18747	(1)	2.21 <sup>+0.25</sup> <sub>-0.22</sub>	-	<0.01	0.608	8%	-		$\mathcal{B}$ ( $n\mathcal{B}$ )
28357	(2)	2.38 <sup>+0.05</sup> <sub>-0.05</sub>	0.10 <sup>+0.01</sup> <sub>-0.01</sub>	<0.01	1.013	15%	0.006	✓	$\mathcal{B}$ ( $n\mathcal{B}$ )
29911	(2)	1.67 <sup>+0.58</sup> <sub>-0.79</sub>	0.22 <sup>+0.09</sup> <sub>-0.06</sub>	<0.01	0.853	15%	0.298	✓	$\mathcal{B}$ ( $n\mathcal{B}$ )
93560*	(1)	2.51 <sup>+0.64</sup> <sub>-0.54</sub>	-	0.25 <sup>+0.20</sup> <sub>-0.16</sub>	1.283*	-	-		$\mathcal{B}$ ( $n\mathcal{B}$ )
115294*	(1)	2.17 <sup>+0.34</sup> <sub>-0.30</sub>	-	<0.01	0.840*	-	-		$\mathcal{B}$ ( $n\mathcal{B}$ )
126294	(2)	2.30 <sup>+0.29</sup> <sub>-0.28</sub>	0.038 <sup>+0.0037</sup> <sub>-0.033</sub>	<0.01	1.14	26%	0.212		$\mathcal{B}$ ( $n\mathcal{B}$ )
155872	(2)	2.03 <sup>+0.48</sup> <sub>-0.43</sub>	0.15 <sup>+0.02</sup> <sub>-0.04</sub>	<0.01	1.106	35%	0.004	✓	$\mathcal{B}$ ( $n\mathcal{B}$ )
282027*	(1)	2.40 <sup>+0.59</sup> <sub>-0.46</sub>	-	<0.01	1.332*	-	-		$\mathcal{B}$ ( $n\mathcal{B}$ )
294033	(2)	2.03 <sup>+0.58</sup> <sub>-0.53</sub>	0.13 <sup>+0.02</sup> <sub>-0.02</sub>	<0.01	0.914	15%	0.052		$\mathcal{B}$ ( $n\mathcal{B}$ )
297574	(2)	2.03 <sup>+0.36</sup> <sub>-0.35</sub>	0.13 <sup>+0.02</sup> <sub>-0.03</sub>	<0.01	0.848	13%	0.0004	✓	$\mathcal{B}$ ( $n\mathcal{B}$ )
321587	(2)	2.21 <sup>+0.13</sup> <sub>-0.13</sub>	0.12 <sup>+0.02</sup> <sub>-0.02</sub>	<0.01	1.033	24%	0.014	✓	$\mathcal{B}$ ( $n\mathcal{B}$ )
324308	(1)	1.98 <sup>+0.11</sup> <sub>-0.10</sub>	-	<0.01	1.064	34%	-		$\mathcal{B}$ ( $n\mathcal{B}$ )
341733	(2)	1.88 <sup>+0.26</sup> <sub>-0.22</sub>	0.14 <sup>+0.03</sup> <sub>-0.06</sub>	<0.01	0.905	14%	0.051		$\mathcal{B}$ ( $n\mathcal{B}$ )
350309	(2)	2.19 <sup>+0.23</sup> <sub>-0.22</sub>	0.09 <sup>+0.02</sup> <sub>-0.02</sub>	<0.01	1.008	24%	0.0003		$\mathcal{B}$ ( $n\mathcal{B}$ )
358675	(2)	1.66 <sup>+0.20</sup> <sub>-0.20</sub>	0.04 <sup>+0.02</sup> <sub>-0.02</sub>	<0.01	1.395	53%	0.029		$\mathcal{B}$ ( $n\mathcal{B}$ )
36405*	(1)	2.29 <sup>+0.28</sup> <sub>-0.26</sub>	-	<0.01	0.770*	-	-		$\mathcal{B}$ ( $n\mathcal{B}$ )
369702	(2)	2.19 <sup>+0.46</sup> <sub>-0.42</sub>	0.12 <sup>+0.05</sup> <sub>-0.06</sub>	<0.01	1.033	18%	1.6 · 10 <sup>-6</sup>		$\mathcal{B}$ ( $n\mathcal{B}$ )
3161*	(1)	0.92 <sup>+0.39</sup> <sub>-0.21</sub>	-	<0.14	0.912*	-	-		$\mathcal{N}$ ( $n\mathcal{N}$ )
3173	(1)	1.74 <sup>+0.43</sup> <sub>-0.37</sub>	-	0.41 <sup>+0.24</sup> <sub>-0.18</sub>	1.056	25%	-	✓	$\mathcal{N}$ ( $n\mathcal{N}$ )
120992*	(1)	1.99 <sup>+1.75</sup> <sub>-1.31</sub>	-	7.11 <sup>+7.29</sup> <sub>-4.42</sub>	0.663*	-	-	✓	$\mathcal{N}$ ( $n\mathcal{N}$ )
155684*	(1)	1.54 <sup>+1.18</sup> <sub>-0.63</sub>	-	<1.81	1.119*	-	-		$\mathcal{N}$ ( $n\mathcal{N}$ )
266064*	(1)	1.22 <sup>+1.51</sup> <sub>-1.17</sub>	-	23.3 <sup>+22.8</sup> <sub>-13.8</sub>	0.971*	-	-		$\mathcal{N}$ ( $n\mathcal{N}$ )
277671*	(1)	0.79 <sup>+0.25</sup> <sub>-0.25</sub>	-	<0.11	0.709*	-	-		$\mathcal{N}$ ( $n\mathcal{N}$ )
348033*	(1)	1.62 <sup>+1.64</sup> <sub>-0.70</sub>	-	<1.61	0.701*	-	-		$\mathcal{N}$ ( $n\mathcal{N}$ )
350410*	(1)	0.97 <sup>+0.57</sup> <sub>-0.42</sub>	-	0.42 <sup>+0.69</sup> <sub>-0.33</sub>	0.723*	-	-	✓	$\mathcal{N}$ ( $n\mathcal{N}$ )
354458*	(1)	1.87 <sup>+0.43</sup> <sub>-0.39</sub>	-	<0.04	1.008*	-	-		$\mathcal{N}$ ( $n\mathcal{N}$ )
1780	(1)	2.47 <sup>+0.51</sup> <sub>-0.45</sub>	-	<0.11	0.914	33%	-		$\mathcal{N}1$ ( $n\mathcal{N}1$ )
28899	(1)	2.92 <sup>+0.26</sup> <sub>-0.23</sub>	-	<0.01	0.536	4%	-		$\mathcal{N}1$ ( $n\mathcal{B}$ )
47793*	(1)	1.96 <sup>+0.43</sup> <sub>-0.36</sub>	-	<0.08	0.669*	-	-		$\mathcal{N}1$ ( $n\mathcal{N}1$ )
88476	(2)	1.94 <sup>+0.30</sup> <sub>-0.30</sub>	0.07 <sup>+0.04</sup> <sub>-0.03</sub>	<0.01	0.508	1%	0.013		$\mathcal{N}1$ ( $n\mathcal{B}$ )
93640	(2)	2.24 <sup>+0.22</sup> <sub>-0.21</sub>	0.016 <sup>+0.078</sup> <sub>-0.006</sub>	<0.05	0.764*	-	0.012		$\mathcal{N}1$ ( $n\mathcal{N}1$ )
266125*	(1)	2.07 <sup>+0.52</sup> <sub>-0.47</sub>	-	<0.26	1.006*	-	-		$\mathcal{N}1$ ( $n\mathcal{N}1$ )
275370*	(1)	6.90 <sup>+</sup> <sub>-4.16</sub>	-	<0.01	0.577*	-	-		$\mathcal{N}1$ ( $n\mathcal{N}1$ )
291676*	(1)	3.02 <sup>+0.63</sup> <sub>-0.36</sub>	-	<0.09	0.958*	-	-		$\mathcal{N}1$ ( $n\mathcal{B}$ )
303293*	(1)	1.71 <sup>+0.46</sup> <sub>-0.38</sub>	-	<0.01	1.029*	-	-		$\mathcal{N}1$ ( $n\mathcal{N}1$ )
305003	(1)	2.33 <sup>+0.12</sup> <sub>-0.11</sub>	-	<0.03	0.839	4%	-		$\mathcal{N}1$ ( $n\mathcal{N}1$ )
337999	(1)	1.83 <sup>+0.28</sup> <sub>-0.25</sub>	-	0.19 <sup>+0.11</sup> <sub>-0.09</sub>	1.241	47%	-		$\mathcal{N}1$ ( $n\mathcal{B}$ )
339379*	(1)	1.07 <sup>+0.40</sup> <sub>-0.38</sub>	-	<0.01	1.089*	-	-		$\mathcal{N}1$ ( $n\mathcal{N}1$ )
356567	(1)	2.66 <sup>+0.13</sup> <sub>-0.12</sub>	-	<0.01	0.826	13%	-		$\mathcal{N}1$ ( $n\mathcal{B}$ )

**Notes.** All quoted errors are for a 90% confidence interval for one parameter. <sup>(1)</sup> The lower limit of 0.1 on  $N_H$  corresponds to the limit imposed by XSPEC. <sup>(2)</sup> The sub-sample names  $\mathcal{B}$ ,  $\mathcal{N}$  and  $\mathcal{N}1$  correspond respectively to the *broad*, *narrow* and *unobscured narrow* sub-samples. The classification given in brackets is discussed later, in section 3.4. <sup>(3)</sup> Very low number of counts (Cash statistic is used instead of  $\chi^2$  statistic), not sufficient to check the presence of a soft excess. <sup>(\*)</sup> Test statistic value when the Cash fit statistic is used. Model (1) corresponds to an absorbed power-law (tbabs\*(zpo\*pha)) and model (2) to a soft excess in addition to an absorbed power-law (tbabs\*((zpo+zbb)\*pha)).

be attributed to the blurred ionized reflection from the inner parts of the accretion disc (Gierliński & Done 2004; Crummy et al. 2006) or to the Comptonization of extreme UV accretion disc photons (Ross et al. 1992). The Fe K $\alpha$  fluorescent

emission-line is a signature of X-ray reprocessing (reflection of the power-law component by a cold disc; accretion disc or torus).

The spectral fitting is performed as follows:

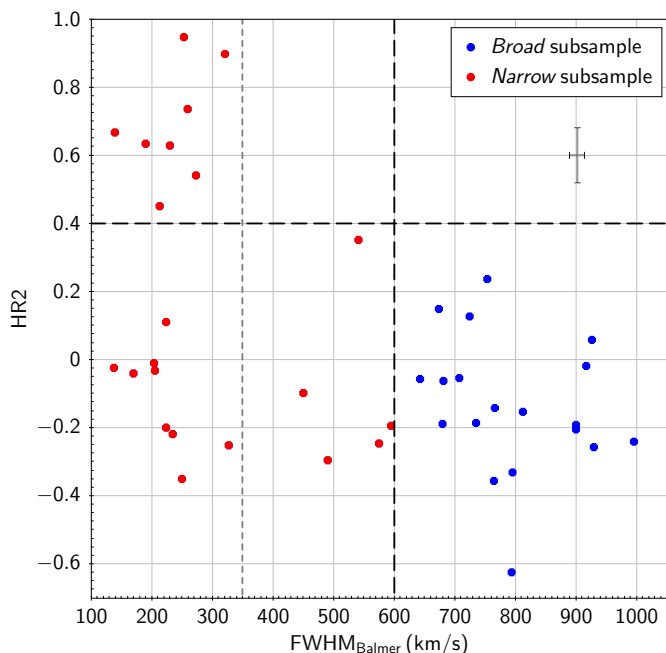


**Fig. 4.** HR2 vs. Balmer velocity width of elusive AGN. A total of 19 sources (blue symbols) do not show clear signs of absorption and have broader line widths; they are NLS1 candidates (*broad* sub-sample). The remaining 22 sources with narrower line widths (red symbols; *narrow* sub-sample) show different properties, only 41% of them exhibit clear signs of absorption. The size of the typical (mean) errors is indicated by the black error-bars shown in the top right of the diagram.

1. We first fit the data in the 2-10 keV energy range with a power-law (zpo model in XSPEC syntax) corrected for foreground absorption in our own Galaxy (tbabs;  $N_{H,gal}$ ) and modified by intrinsic absorption (pha;  $N_H$ ). The  $N_{H,gal}$  parameter is fixed to the value computed using the emphnhftool (see Table 1), while  $N_H$  is free to vary.
2. We then check for the presence of an additional Fe emission line around 6.4 keV, which can be modelled by a component with a Gaussian profile (zgauss).
3. We finally include the data between 0.3 and 2 keV to see if these data are in excess compared to the previously fitted power-law. If this is the case, we add a blackbody component (zbody) to model the soft excess.

The best fit model is the one that gives the smallest reduced- $\chi^2$  ( $= \chi^2/d.o.f.$ ). When the best fit model is the combination of 2 components (i.e. an absorbed power-law plus a soft excess and/or a Fe line), we use the XSPEC *Ftest* task to determine whether the inclusion of an additional component is needed. We also check the validity of the model using the XSPEC *goodness* parameter which returns the percentage of simulations for which the statistic is less than that for the observed data; so a smaller *goodness* parameter values indicates a better model (but this can only be used for  $\chi^2$  statistic). We choose to keep the additional component if the F-test probability  $P(f_{test}) < 10^{-2}$ , or if the *goodness* parameter is really improved (i.e. a parameter difference of at least 20%).

The results of the spectral fitting are given Table 2. In the case of very low quality spectra, the number of counts was not sufficient to check the presence of a soft excess. Two example spectra (one for a source from the emphbroad sub-sample and one from the *narrow* sub-sample) are shown in Fig.5.

A Seyfert galaxy is expected to have a photon index of about 1.8 (Nandra et al. 1997), while NLS1 have a softer X-ray slope,

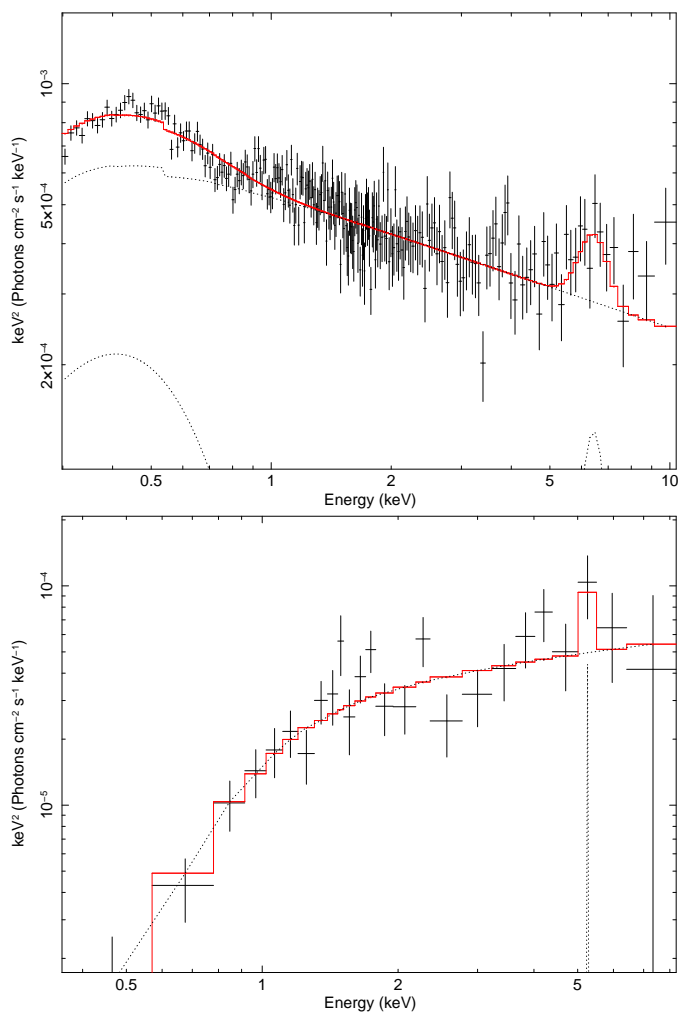


**Fig. 5.** Example X-ray spectra. **Upper panel:** NLS1 candidate (SRCID 28357) fitted with a power-law plus a blackbody component for the soft excess and a Gaussian component for the Fe line. **Lower panel:** a *narrow* source (SRCID 3173) fitted with a Gaussian component (Fe line) in addition to an absorbed power law. The dashed lines represent the separate model components while the red line is the resulting best fit model.

steeper than that of classical Seyferts (Botte et al. 2004). The sources from the *broad* sub-sample (i.e. NLS1 candidates) have a photon index  $\Gamma$  consistent with what is expected for NLS1 ( $\Gamma > 1.8$ ) and have no or little intrinsic absorption ( $N_H < 4 \cdot 10^{21} \text{ cm}^{-2}$  is often taken to be the separation between absorbed and unabsorbed AGNs; Caccianiga et al. (2007)); strongly supporting their classification. The sources from the *narrow* sub-sample, with high HR2 ( $> 0.4$ ), have  $\Gamma < 1.8$  and show signs of absorption in their spectra, so their X-ray emission resemble that of classical Seyfert 2 (Sy2) galaxies; while the others (*unobscured narrow* sub-sample) have a  $\Gamma \gtrsim 1.8$  and their X-ray spectra alone cannot distinguish between NLS1 and Sy2 (see Fig. 6). The X-ray spectral analysis nevertheless confirms that the sample sources with a low HR do not show signs of absorption or have little intrinsic absorption.

#### 3.4. Forbidden vs. permitted lines width

To better distinguish between Sy2 and NLS1 (especially for the sources from the *unobscured narrow* group with  $\Gamma \sim 1.8$ ), we examine one of the NLS1 properties, the emission line width.

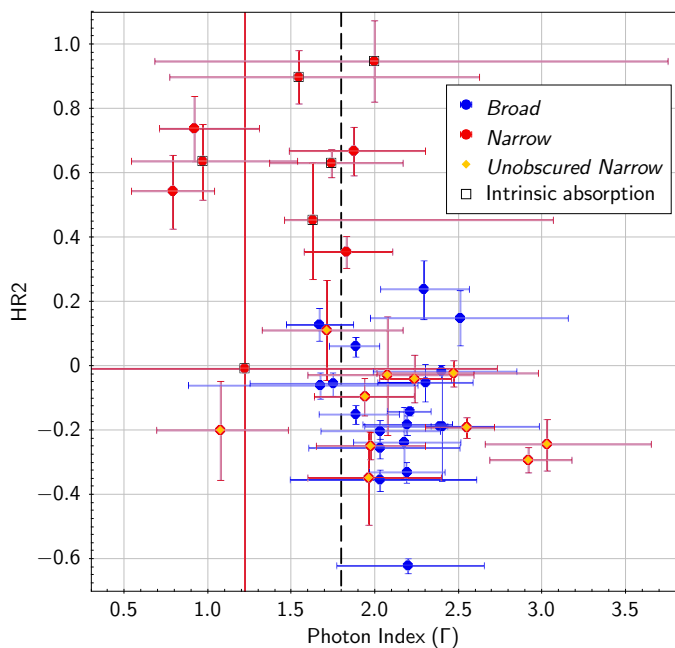


**Fig. 6.** HR2 vs. X-ray photon index. NLS1 candidates (in blue) have  $\Gamma$  mostly larger than 1.8 and are unabsorbed, as expected. For narrow-line sources (in red), some have typical properties of Seyfert 2 ( $\Gamma < 1.8$  and intrinsic absorption) while the others, with low HR2, cannot be clearly classified using their photon index. One of the sources with very large photon index value and error is not plotted.

Because in NLS1 the broad lines come from the BLR, which is presumed to be closer to the BH than the NLR, they have permitted line widths larger than for the forbidden lines (Botte et al. 2004). As we can see in Fig. 7 there are clearly two kinds of sources. Some have the same line width for the permitted and forbidden lines (these we call the *X-ray Seyfert 2* class; 41%) whilst others have larger permitted line widths compared to their forbidden lines (*NLS1* class; 59%). The *NLS1* class, (referring to  $n\mathcal{B}$  in Tables 1 and 2), consists of all the sources from the *broad* sub-sample (i.e. NLS1 candidates) plus the five sources of the *unobscured narrow* sub-sample which have Balmer velocity line width not dominated by the host galaxy. The *X-ray Sy2* sources (named as  $n\mathcal{N}$  in Tables 1 and 2) are the new *narrow* sources, with 8 of them having a low HR ( $n\mathcal{N}1$  classification in Tables 1 and 2, hereafter called *unobscured X-ray Sy2*) and so seem to be unabsorbed.

### 3.5. NLS1 class: Black hole mass and Eddington ratio

To confirm the classification of the NLS1 sources, we compute their BH masses and Eddington ratios ( $\lambda = L_{bol}/L_{Edd}$ ). NLS1 are known to be AGN with very low mass BH and must accrete at near-Eddington rates ( $\lambda \gtrsim 0.25$ ; (Netzer & Trakhtenbrot 2007)) in order to maintain an AGN-like luminosity.

NLS1 share the same stellar velocity dispersion range as type 1 AGN in the  $M_{BH} - \sigma$  relation (Botte et al. 2004), so we can use the same BH mass relation as for unobscured AGN to estimate the mass of their central object. The mass of a BH can be computed assuming virial equilibrium:  $M_{BH} = R_{BLR}v^2G^{-1}$ . We use the scaling relation of Xiao et al. (2011):

$$M_{BH} (M_{\odot}) = 3.47 \cdot \left[ \frac{\lambda L_{5100\text{\AA}}}{10^{44} \text{ erg.s}^{-1}} \right]^{0.519} \cdot \left[ \frac{FWHM_{H\alpha}}{\text{km.s}^{-1}} \right]^{2.06} \quad (1)$$

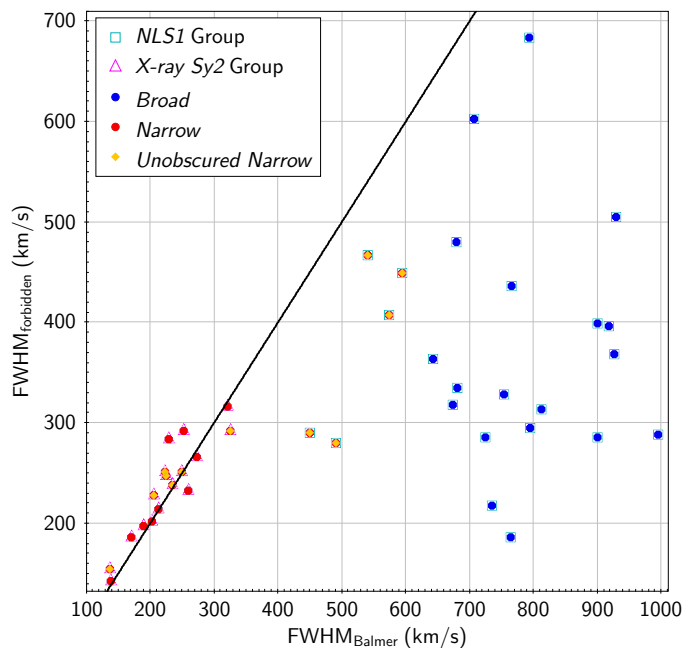


**Fig. 7.** Forbidden vs. permitted line widths. The black line corresponds to equal width. This comparison is used to distinguish between *X-ray Sy2* (sources with equal line width) and *NLS1* (which consists of all the *broad* sources (blue symbols) plus 5 sources from the *unobscured narrow* group).

In this relationship, the size of the BLR, ( $R_{BLR}$ ), is inferred from the AGN continuum luminosity at  $5100\text{\AA}$  using the revised relation from Bentz et al. (2009) calibrated using  $H\beta$ . Then  $FWHM_{H\beta}$  is converted to  $FWHM_{H\alpha}$  according to the empirical relationship derived in Greene & Ho (2005). Finally Xiao et al. (2011) assume an isotropic distribution of orbits with random inclinations ( $v = f \cdot FWHM = \sqrt{3}/2 \cdot FWHM$ ). The luminosity  $\lambda L_{5100}$  is the rest-frame luminosity corrected for Galactic absorption and host galaxy stellar contribution. The FWHM measurement for my sample comes from the SDSS GALSPEC spectral products and corresponds to the value fitted simultaneously for all of the Balmer lines.

The Eddington ratio only depends on the Eddington luminosity  $L_{Edd}$  and on the bolometric luminosity  $L_{bol}$ . The Eddington luminosity is directly linked to the BH mass:

$$L_{Edd} = 1.25 \cdot 10^{38} \left( \frac{M_{BH}}{M_{\odot}} \right) \text{ erg.s}^{-1} \quad (2)$$

Because our sample have low [OIII] luminosities for AGN and the MIR emission can be contaminated by SF, the best choice to compute the bolometric luminosity is to use the hard X-ray luminosity ( $L_{bol} = L_{HX} \cdot C_{HX}$ ). The conversion factor  $C_{HX}$  depends on  $L_{HX}$  (Vasudevan & Fabian 2007) and can be estimated using the relation from Marconi et al. (2004):

$$\log \left( \frac{L_{bol}}{L_{HX}} \right) = 1.54 + 0.24\mathcal{L} + 0.012\mathcal{L}^2 - 0.0015\mathcal{L}^3 \quad (3)$$

where  $\mathcal{L} = \log(L_{bol}) - 12$ , and  $L_{bol}$ ,  $L_{HX}$  are in units of  $L_{\odot}$ .

Using equations (1), (2) and (3), the sources from the *NLS1* group have low mass BH ( $M_{BH} < 5 \cdot 10^6 M_{\odot}$ ); compared to a typical AGN which has  $M_{BH} \sim 10^7 - 10^9 M_{\odot}$ ; and also have a high Eddington ratio ( $\lambda \gtrsim 0.25$ ) as expected, as shown in Fig. 8.

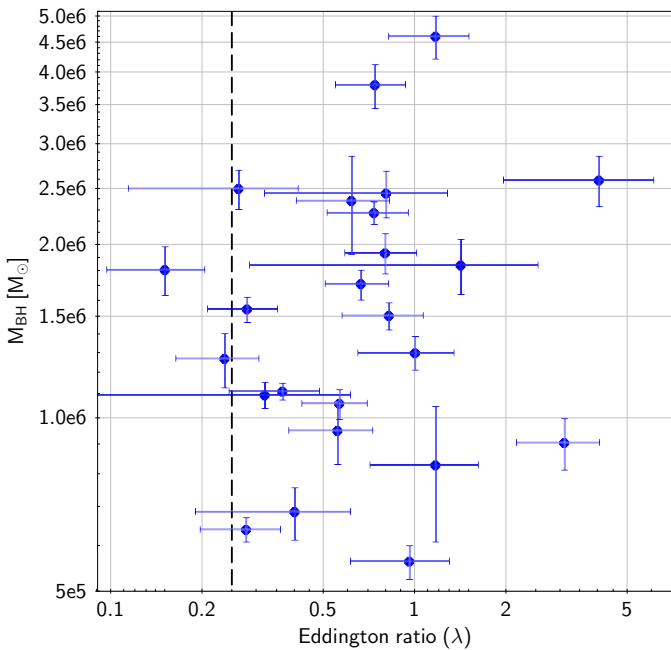


**Fig. 8.**  $M_{BH}$  and Eddington ratio for the NLS1. The dashed line represents the lower limit to the observed Eddington ratio for NLS1 ( $\lambda_{NLS1,lim} = 0.25$ ).

Among the elusive AGN, half of sources (59%) are likely to be NLS1 and are optically misclassified as star-forming galaxies due to the fact that Balmer lines ( $H\alpha$  and  $H\beta$ ) come from both the NLR and BLR regions and therefore cannot be correctly classified using the BPT diagram. However, we still have 41% of the sample that do not appear to be NLS1, and mostly resemble X-ray type 2 AGN, in the sense that they do not possess optical broad lines and have AGN X-ray luminosity (in contrast with the work of Castelló-Mor et al. (2012) who found that the population of elusive AGN is entirely comprised of NLS1). Possible reasons of their optical misclassification are discussed in the next section.

#### 4. Why type 2 AGN could be optically misclassified as SF galaxies

We consider three possible explanations for the fact that the X-ray Sy2 galaxies (i.e. the 17 sources with  $FWHM_{Balmer} < 400 \text{ km.s}^{-1}$ ) are not apparent as AGN in the optical band: obscuration, optical dilution by host galaxy starlight and weak emission from the AGN.

##### 4.1. Obscuration hypothesis

In order to explain the optical dullness of the sources with obscuration, we need to consider complete obscuration of the central engine and/or the NLR. One possibility is that the nuclear absorber is not distributed in the torus-like geometry assumed for the classical model, and so obscuration may be caused by spherical Compton-thick gas clouds, covering almost  $4\pi$  at the central engine (Comastri et al. 2002; Civano et al. 2007), implying that ionising photons cannot escape from the nuclear source to produce the NLR. Or, if the covering of the nuclear source is not complete, only few photons can reach the NLR, leading to attenuated emission lines from this region. On the other hand, Rigby et al. (2006) proposed the presence of extranuclear dust and gas.

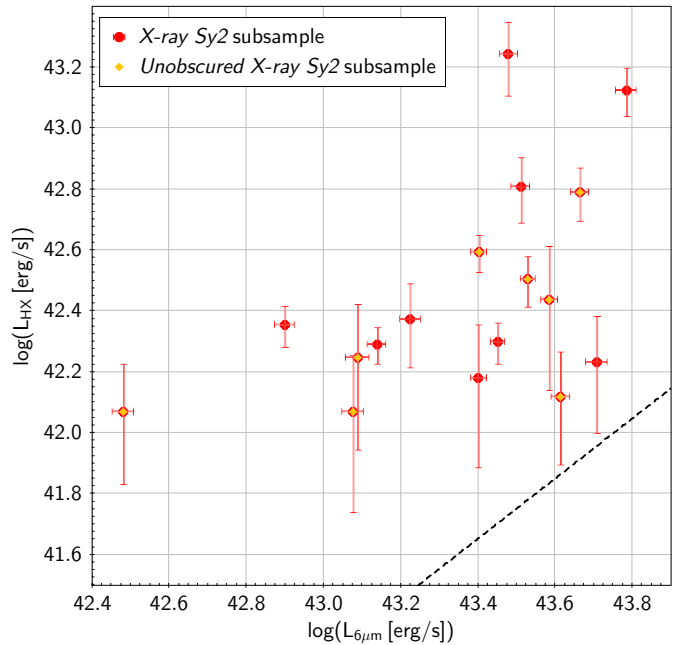


**Fig. 9.** Comparison of the  $L_{HX}$  and  $L_{6\mu m}$ , two indirect AGN luminosity indicators, confirming the absence of Compton-thick sources. The Compton-thick region on the diagram lies below the black dashed line.

These are distributed on large scales (i.e. dust lanes) in the host galaxy along our line of sight and which may hide the emission lines from the NLR.

According to the X-ray spectral fitting results (see section 3.3), the hydrogen column density  $N_H$  is, for almost all of the sources, much smaller than  $10^{22} \text{ cm}^{-2}$ , corresponding to an optical extinction value  $A_V \ll 4.5 \text{ mag}$  (assuming the Galactic relation:  $A_V = 4.5 \cdot 10^{-22} N_H$  of Güver & Özel (2009)), and so are not heavily absorbed.

For AGN with column density greater than  $> 10^{24} \text{ cm}^{-2}$ , X-rays are significantly absorbed and scattered above a few keV, so X-ray spectra below 10 keV do not provide information on the real column density. The possibility that some sources are Compton-thick can be investigated by evaluating the total absorption by comparing two indirect AGN luminosities. The  $6\mu m$  continuum luminosity is a good proxy for the AGN luminosity, like the hard X-ray luminosity. We estimate the  $6\mu m$  flux, and thus luminosity, from the WISE fluxes in the four bands ( $3.4\mu m$ ,  $4.6\mu m$ ,  $12\mu m$  and  $24\mu m$ ) using a weighted linear least square fitting (e.g.  $\log f_\nu \propto \log \lambda$ ). This analysis, see Fig. 9, confirms that all of the sources lie above the Compton-thick region of the diagram (Goulding et al. 2011).

We can conclude that obscuration of the central BH is unlikely to be the cause of the elusiveness of optical AGN signatures in these sources. Moreover, the absence of observed obscuration in the sources with narrow emission lines (i.e. *unobscured X-ray Sy2*) is not due to Compton-thick absorbers, which can be confirmed by comparing the [OIII] and hard X-ray luminosities. In the presence of high levels of absorption, the hard X-ray luminosity is expected to be depressed by an amount related to the absorbing column density, while the [OIII] emission, coming from the NLR, should be unaffected. Compton-thick sources ( $N_H > 10^{24} \text{ cm}^{-2}$ ) are expected to have a thickness parameter  $T = L_{HX}/L_{[OIII]}$  smaller than 0.1 (i.e.  $\log T < -1$ ) (Bassani et al. 1999). The X-ray Sy2 class in this sample have  $\log T$  between 0.5 and 2.5 (see Fig. 2), so do not appear to be Compton-thick sources.

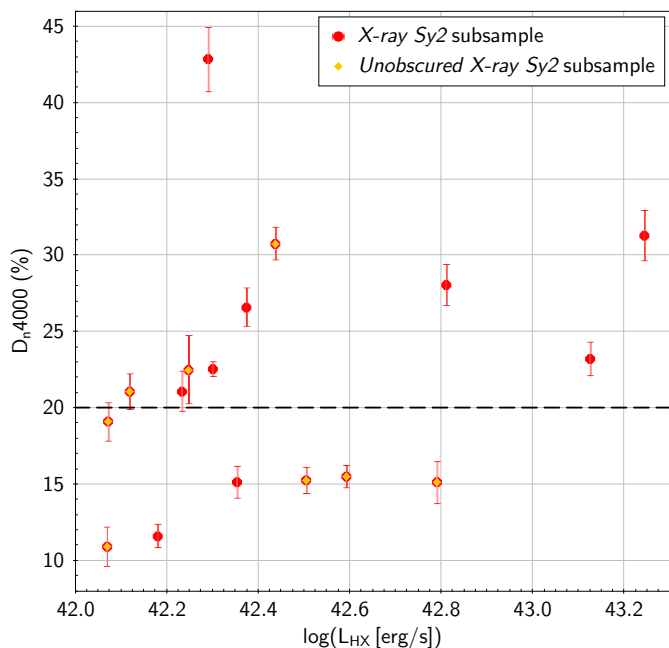


**Fig. 10.** 4000Å break ( $\Delta_n$ ) values for the sources in the *X-ray Sy2* group. The optical continuum of a galaxy is dominated by AGN for  $\Delta_n < 20\%$ , and for larger values it is dominated by the host galaxy light.

#### 4.2. Optical dilution hypothesis

Another possible explanation for the absence of an AGN signature in the optical spectrum of these sources is the optical dilution of the AGN activity by starlight from the host galaxy, with a possible additional star-formation contribution.

The contribution of starlight from the host galaxy can be estimated using the 4000Å break ( $\Delta_n$ ):

$$\Delta_n = \frac{F^+ - F^-}{F^+}$$

where  $F^+$  and  $F^-$  represent the mean value of the flux density in the rest-frame regions 4000-4100Å and 3850-3950Å respectively (definition from Balogh et al. (1999), less sensitive to reddening by dust). The nuclear emission is dominant if the value of  $\Delta_n$  is below 20%, whilst the host galaxy light dominates the continuum if  $\Delta_n$  ranges from 20% to 60%. For  $\Delta_n$  values between 20%-40% both the AGN and the host galaxy contribute to the spectrum.

We can see in Fig. 10 that 10 of the 17 *X-ray Sy2* sources have their blue continuum dominated by the host galaxy starlight and so the AGN light is diluted.

Moreover, by comparing the observed  $H\alpha$  line luminosity with the value expected for an AGN (using the relation from Panessa et al. (2006)), most of these sources have Balmer emission lines fluxes in excess, which could be due to star-formation. Any star-formation contribution will enhance the Balmer lines and so reduce the  $[OIII]/H\beta$  and  $[NII]/H\alpha$  line ratios, moving the sources from the AGN region to the SF region of the BPT diagram.

So intrinsic weakness of the AGN, in respect to the host galaxy, combined in some cases with a star-formation contribution could explain the elusiveness of about 60% of the sources of the *X-ray Sy2* group.

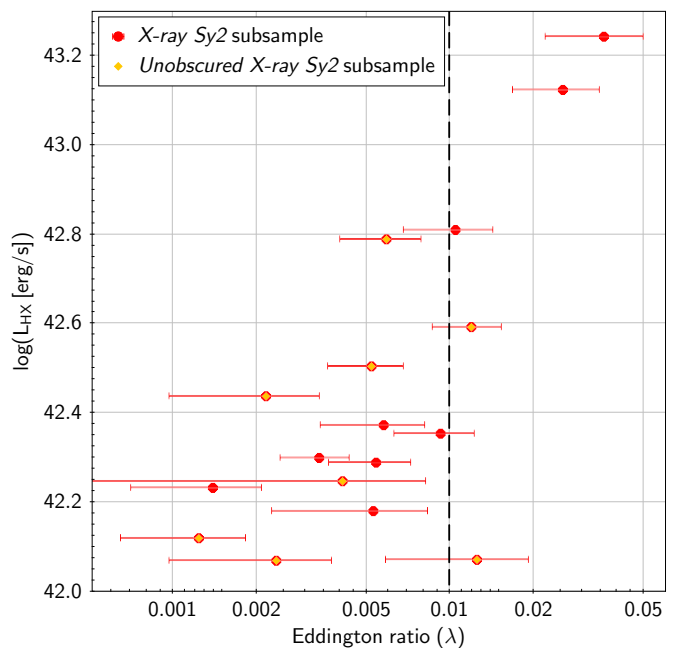


**Fig. 11.** Hard X-ray luminosity vs. Eddington ratio ( $\lambda$ ) of the *X-ray Sy2* sources. The values of  $\lambda$  are low compared to typical AGN and the low HR2 sources (in yellow) have very low accretion rates ( $\lambda < 10^{-2}$ ; black dash line) and so are good candidates to be *True Sy2*.

#### 4.3. Low accretion rate hypothesis

Finally, undiluted optically dull AGN could be characterised by intrinsically weak optical emission from the accretion disk. In the case of low accretion rates, AGN are expected to be optically underluminous compared with typical AGN due to radiatively inefficient accretion flows (RIAFs, Yuan & Narayan (2004)).

The Eddington ratio ( $\lambda = L_{bol}/L_{Edd}$ ) of these sources is computed using the equations (2) and (3) described in the section 3.5 for the bolometric luminosity. The BH masses of the Sy2 sources were estimated using the relation between  $M_{BH}$  and the rest-frame K-band bulge luminosity (from Graham (2007), as improved by Trump et al. (2011)):

$$\log\left(\frac{M_{BH}}{M_{\odot}}\right) = 0.93 \cdot (\log(L_{K,bulge}) - 0.3z) + 32.30$$

with  $L_{K,bulge}$  in  $\text{erg}\cdot\text{s}^{-1}$  and  $L_{K,bulge} = 0.5 \cdot L_{K,host}$  assumed for narrow-line AGN.

As can be seen in Fig. 11, the Sy2 sources have low Eddington ratios,  $0.001 < \lambda < 0.05$ , compared to typical AGN ( $\lambda \sim 0.07 - 1$ , Heckman et al. (2004)), providing an explanation for the optical elusiveness of these sources. Moreover, all the *unobscured X-ray Sy2* sources have very low accretion rates ( $\lambda < 10^{-2}$ ). A recent study by Trump et al. (2011) showed that for a specific accretion rates ( $\lambda < 10^{-2}$ ), the BLR disappears because of the occurrence of a RIAF extending to the inner region of the accretion disk. Below this specific accretion rate, the disk wind, which is supposed to form in the BLR, is no longer supported. The resulting AGN are unobscured but lack broad emission lines in their optical spectrum: they are called *True Sy2*.

Therefore, the 8 *unobscured X-ray Sy2* sources are good candidates to be *True Sy2* AGN.



#### 4.4. True Sy2 candidates: Expected FWHM and luminosity of the broad lines

True Sy2 candidates have no intrinsic absorption so, according to the Unified Model, are expected to exhibit broad optical emission lines. To confirm their classification as True Sy2, we can compute their expected BL FWHM and luminosity and compare these with the observed values.

For the broad H $\alpha$  line, the FWHM is directly related to the BH mass and continuum luminosity at 5100Å (see equation (1), section 3.5).

The predicted broad H $\alpha$  luminosity can be estimated from the empirical relation of Greene & Ho (2005):

$$L_{Broad\ H\alpha} = (5.25 \pm 0.02) \cdot 10^{42} \left( \frac{\lambda L_{5100}}{10^{44} \text{ erg.s}^{-1}} \right)^{(1.157 \pm 0.005)} \text{ erg.s}^{-1}$$

The rms scatter in this relation is quite small, being  $\sim 0.2$  dex.

The observed flux and line width of H $\alpha$ , from the optical spectrum, and the predicted values for the broad component from the equations above and (1), are given Table 3.

The observed spectrum in the H $\alpha$  region with the predicted broad H $\alpha$  component superimposed is shown in Fig. 12. The H $\alpha$  line is fitted with a Gaussian profile. The predicted broad component is modelled by Gaussian function with width and flux as discussed above; the predicted component is plotted with randomised measurement noise equivalent to that of the actual observed spectrum. The broad line flux plotted in Fig. 12 is the fitted value (SRCIDs 1780, 93640, 305003) where a possible weak line is detected or, if no line is detected, an upper limit, set to twice the apparent noise level (see Table 3, column 3).

We can then compare the predicted and measured parameters for H $\alpha$ . We can see Fig. 13 that there is a large difference between the predicted and measured (or upper limit) fluxes of the broad H $\alpha$  component. For a consistent observed flux with the prediction, we expect a value of  $\Delta$  (with  $\Delta = f_{BroadH\alpha, predicted} - f_{BroadH\alpha, measured}$ ) around 0. However, we can see that the minimum  $\Delta$ , even if considering the errors, is about 1000 (with a mean value  $\sim 2000$ ), so far away from the expected value of 0. Thus, there is no chance that the observed flux was consistent with the predicted value for the broad H $\alpha$  line. The observed, or upper limit, broad component flux constitutes only 0.5 to 2.4% of the predicted flux. Moreover, these sources have an observed broad H $\alpha$  flux  $\gtrsim 1$  dex lower than the predicted value. While the scatter in the Greene & Ho (2005)  $L_{Broad\ H\alpha} - \lambda L_{5100}$  relation, due to the intrinsic scatter of QSO properties, is only  $\sim 0.2$  dex; so the observed difference between the observed and predicted fluxed is a real effect. We thus conclude that a broad H $\alpha$  line

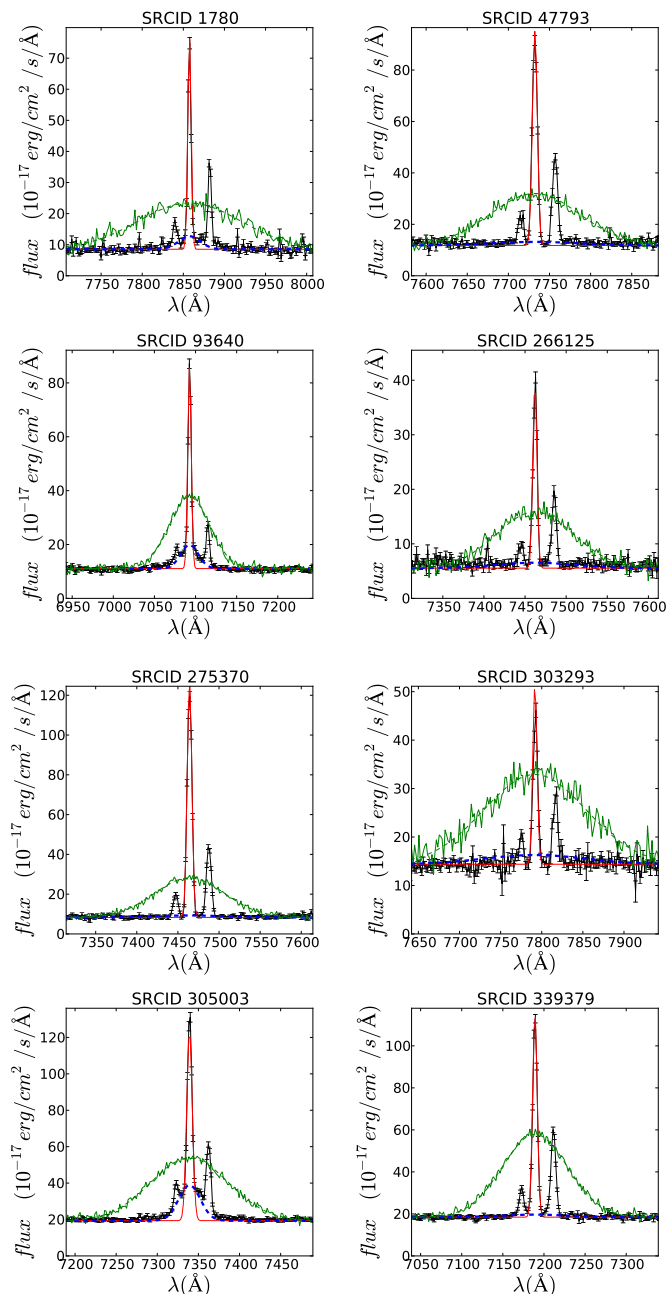


**Fig. 12.** Optical spectra of the True Sy2 candidates around the H $\alpha$  region. The observed H $\alpha$  line is fitted with a Gaussian profile (red curve) while the predicted broad component is represented by a Gaussian (green). The dashed blue line represents the fitted weak broad line or the upper limit to the broad component.

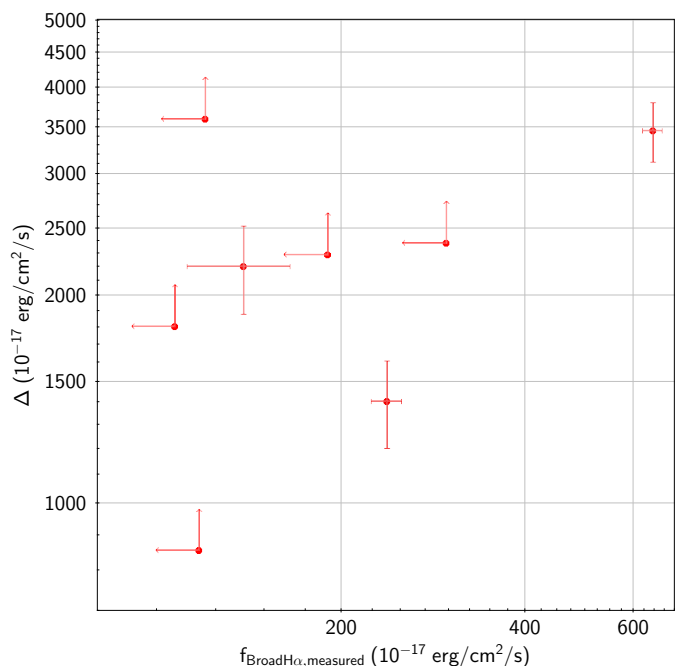


**Fig. 13.** Difference between the predicted and measured flux (noted as  $\Delta$ ) vs. measured flux for the H $\alpha$  broad component of the True Sy2 candidates.

**Table 3.** True Sy2: observed and predicted parameters for H $\alpha$ .

SRCID	Narrow H $\alpha$ <sup>1</sup>		Broad H $\alpha$ <sup>2</sup>		Predicted Broad H $\alpha$ <sup>3</sup>	
	<i>flux</i> <sup>a</sup>	<i>FWHM</i> <sup>b</sup>	<i>flux</i> <sup>a</sup>	<i>FWHM</i> <sup>b,*</sup>	<i>flux</i> <sup>a</sup>	<i>FWHM</i> <sup>b</sup>
1780	357 ± 6	188 ± 3	139 ± 26	1181 ± 430	2338 ± 295	5638 ± 375
47793	631 ± 8	275 ± 3	<190	4940	2741 ± 264	4940 ± 286
93640	398 ± 5	212 ± 2	238 ± 14	1071 ± 278	1642 ± 190	2454 ± 279
266125	216 ± 4	242 ± 4	<117	4428	1210 ± 238	4428 ± 1769
275370	843 ± 9	266 ± 2	<107	4047	2130 ± 221	4047 ± 246
303293	243 ± 43	237 ± 16	<296	5638	2887 ± 209	5638 ± 303
305003	887 ± 9	327 ± 3	644 ± 23	1265 ± 268	4099 ± 318	4579 ± 177
339379	691 ± 7	280 ± 2	<119	3915	3934 ± 222	3915 ± 155

**Notes.** <sup>(1)</sup> Parameters from the optical spectrum, obtained by the SDSS line fitting pipeline (SDSS *SpecLine* table) (Fig. 12 red curve). <sup>(2)</sup> Fitted weak line (SRCIDs 1780, 93640, 305003) or the upper limit of the broad component (Fig. 12 dashed blue line). <sup>(3)</sup> Predicted broad H $\alpha$  component computed using equations of Section 4.4 (Fig. 12 green curve).

<sup>(a)</sup> Line flux in units of  $10^{-17}$  erg/cm<sup>2</sup>/s. <sup>(b)</sup> Full Width at Half Maximum in units of km.s<sup>-1</sup>. <sup>(\*)</sup> The FWHM of the broad component is the fitted value when a weak broad line is present, otherwise it is fixed at the predicted value (column 7 of the table).

would have been securely detected if present at the expected level. In conclusion these sources clearly lack broad lines and seem to be True Sy2.

## 5. Summary and conclusions

We have investigated the nature of a sample of X-ray selected AGN optically (mis)classified as SF galaxies in the BPT diagnostic diagram (elusive AGN), and have discussed possible reasons for the misclassification. For this purpose, we have looked at their optical and X-ray properties.

We find that 59% of the elusive AGN are very likely to be NLS1, showing a steep X-ray spectrum with no intrinsic absorption consistent with a low hardness ratio, forbidden line widths smaller than the Balmer line widths and a high Eddington ratio with low mass black hole. It thus seems that these sources are misclassified in the optical as SF galaxies because of the additional contribution to the Balmer line flux from the BLR and NLR; while the BPT diagram classification assumes contributions only from the NLR.

The other 41% of the remaining elusive AGN have the some properties of type 2 AGN, they have only narrow emission lines in their optical spectra, X-ray luminosity of an AGN but some of them show no sign of absorption (or little absorption), it is that why we call them *X-ray Sy2*. Three possible explanations for their optical elusiveness have been investigated. Heavy obscuration by gas and dust is not a likely origin of the misclassification. However, two other possibilities could explain the optical elusiveness of these sources. Firstly, 60% of them are optically diluted by starlight (so are weak AGN compared to the host galaxy) with a possible star-formation contribution in some cases. Secondly, the *X-ray Sy2* sources also have low accretion rates and are thus optically underluminous due to an intrinsic weakness of the AGN.

Moreover, among these *X-ray Sy2*, we find a population of True Sy2, e.g. undiluted AGN but with a lack of broad emission lines in their optical spectra. The absence of broad lines has been checked by comparing the observed optical spectra with the predicted flux and width of the H $\alpha$  broad component. According to some theoretical models, their very low accretion rates cause the disappearance of the BLR.

*Acknowledgements.* We would like to thank Andrew Blain and Gordon Stewart, together with the referee, Jonathan Trump, for their useful comments. This work uses data from observations obtained with XMM-Newton, an ESA science mission with instruments and contributions directly funded by ESA Mem-

ber States and NASA. Data from the SDSS is also utilised. Funding for SDSS-III has been provided by the Alfred P. Sloan Foundation, the Participating Institutions, the National Science Foundation, and the U.S. Department of Energy Office of Science. The SDSS-III web site is <http://www.sdss3.org/>. This publication also makes use of data products from the Wide-field Infrared Survey Explorer, which is a joint project of the University of California, Los Angeles, and the Jet Propulsion Laboratory/California Institute of Technology, funded by the National Aeronautics and Space Administration.

## References

- Antonucci, R. 1993, ARA&A, 31, 473  
 Baldwin, J. A., Phillips, M. M., & Terlevich, R. 1981, PASP, 93, 5  
 Balogh, M. L., Morris, S. L., Yee, H. K. C., Carlberg, R. G., & Ellingson, E. 1999, ApJ, 527, 54  
 Barth, A. J., Ho, L. C., Rutledge, R. E., & Sargent, W. L. W. 2004, ApJ, 607, 90  
 Bassani, L., Dadina, M., Maiolino, R., et al. 1999, ApJS, 121, 473  
 Bentz, M. C., Peterson, B. M., Netzer, H., Pogge, R. W., & Vestergaard, M. 2009, ApJ, 697, 160  
 Bianchi, S., Panessa, F., Barcons, X., et al. 2012, MNRAS, 426, 3225  
 Boller, T., Brandt, W. N., & Fink, H. 1996, A&A, 305, 53  
 Botte, V., Ciroi, S., Rafanelli, P., & Di Mille, F. 2004, AJ, 127, 3168  
 Brinchmann, J., Charlot, S., White, S. D. M., et al. 2004, MNRAS, 351, 1151  
 Caccianiga, A., Severgnini, P., Della Ceca, R., et al. 2007, A&A, 470, 557  
 Caccianiga, A., Severgnini, P., Della Ceca, R., et al. 2008, A&A, 477, 735  
 Cash, W. 1979, ApJ, 228, 939  
 Castelló-Mor, N., Barcons, X., Ballo, L., et al. 2012, A&A, 544, A48  
 Civano, F., Mignoli, M., Comastri, A., et al. 2007, A&A, 476, 1223  
 Comastri, A., Mignoli, M., Ciliegi, P., et al. 2002, ApJ, 571, 771  
 Crummy, J., Fabian, A. C., Gallo, L., & Ross, R. R. 2006, MNRAS, 365, 1067  
 Elvis, M., Schreier, E. J., Tonry, J., Davis, M., & Huchra, J. P. 1981, ApJ, 246, 20  
 Fabbiano, G. 1989, ARA&A, 27, 87  
 Filippenko, A. V. & Ho, L. C. 2003, ApJ, 588, L13  
 Gierliński, M. & Done, C. 2004, MNRAS, 349, L7  
 Goulding, A. D., Alexander, D. M., Mullaney, J. R., et al. 2011, MNRAS, 411, 1231  
 Graham, A. W. 2007, MNRAS, 379, 711  
 Greene, J. E. & Ho, L. C. 2005, ApJ, 630, 122  
 Güver, T. & Özel, F. 2009, MNRAS, 400, 2050  
 Heckman, T. M., Kauffmann, G., Brinchmann, J., et al. 2004, ApJ, 613, 109  
 Kauffmann, G., Heckman, T. M., Tremonti, C., et al. 2003a, MNRAS, 346, 1055  
 Kauffmann, G., Heckman, T. M., White, S. D. M., et al. 2003b, MNRAS, 341, 33  
 Kewley, L. J., Dopita, M. A., Sutherland, R. S., Heisler, C. A., & Trevena, J. 2001, ApJ, 556, 121  
 Kormendy, J. & Richstone, D. 1995, ARA&A, 33, 581  
 La Franca, F., Fiore, F., Vignali, C., et al. 2002, ApJ, 570, 100  
 Marconi, A., Risaliti, G., Gilli, R., et al. 2004, MNRAS, 351, 169  
 Moran, E. C., Filippenko, A. V., & Chornock, R. 2002, ApJ, 579, L71  
 Mushotzky, R. 2004, in Astrophysics and Space Science Library, Vol. 308, Supermassive Black Holes in the Distant Universe, ed. A. J. Barger, 53  
 Nandra, K., George, I. M., Mushotzky, R. F., Turner, T. J., & Yaqoob, T. 1997, ApJ, 476, 70

- Netzer, H. & Trakhtenbrot, B. 2007, *ApJ*, 654, 754
- Osterbrock, D. E. & Ferland, G. J. 2006, *Astrophysics of gaseous nebulae and active galactic nuclei*
- Osterbrock, D. E. & Pogge, R. W. 1985, *ApJ*, 297, 166
- Panessa, F., Bassani, L., Cappi, M., et al. 2006, *A&A*, 455, 173
- Pineau, F.-X., Motch, C., Carrera, F., et al. 2011, *A&A*, 527, A126
- Ranalli, P., Comastri, A., & Setti, G. 2003, *A&A*, 399, 39
- Reines, A. E., Sivakoff, G. R., Johnson, K. E., & Brogan, C. L. 2011, *Nature*, 470, 66
- Rigby, J. R., Rieke, G. H., Donley, J. L., Alonso-Herrero, A., & Pérez-González, P. G. 2006, *ApJ*, 645, 115
- Rodríguez-Ardila, A., Binette, L., Pastoriza, M. G., & Donzelli, C. J. 2000, *ApJ*, 538, 581
- Ross, R. R., Fabian, A. C., & Mineshige, S. 1992, *MNRAS*, 258, 189
- Schlegel, D. J., Finkbeiner, D. P., & Davis, M. 1998, *ApJ*, 500, 525
- Stasińska, G., Cid Fernandes, R., Mateus, A., Sodré, L., & Asari, N. V. 2006, *MNRAS*, 371, 972
- Tremonti, C. A., Heckman, T. M., Kauffmann, G., et al. 2004, *ApJ*, 613, 898
- Trouille, L. & Barger, A. J. 2010, *ApJ*, 722, 212
- Trump, J. R., Impey, C. D., Kelly, B. C., et al. 2011, *ApJ*, 733, 60
- Trump, J. R., Impey, C. D., Taniguchi, Y., et al. 2009, *ApJ*, 706, 797
- Urry, C. M. & Padovani, P. 1995, *PASP*, 107, 803
- Vasudevan, R. V. & Fabian, A. C. 2007, *MNRAS*, 381, 1235
- Wang, J. X., Malhotra, S., Rhoads, J. E., & Norman, C. A. 2004, *ApJ*, 612, L109
- Watson, M. G., Schröder, A. C., Fyfe, D., et al. 2009, *A&A*, 493, 339
- Xiao, T., Barth, A. J., Greene, J. E., et al. 2011, *ApJ*, 739, 28
- Yuan, F. 2007, in *Astronomical Society of the Pacific Conference Series*, Vol. 373, *The Central Engine of Active Galactic Nuclei*, ed. L. C. Ho & J.-W. Wang, 95
- Yuan, F. & Narayan, R. 2004, *ApJ*, 612, 724
- Zoghbi, A., Fabian, A. C., & Gallo, L. C. 2008, *MNRAS*, 391, 2003